Rationalising the role of solid-acid sites in the design of versatile single-site heterogeneous catalysts for targeted acid-catalysed transformations

Gianotti, Enrica; Manzoli, Maela; Potter, Matthew E.; Shetti, Vasudev N.; Sun, Danni; Paterson, James; Mezza, Thomas M.; Levy, Alan; Raja, Robert. Rationalising the role of solid-acid sites in the design of versatile single-site heterogeneous catalysts for targeted acid-catalysed transformations. CHEMICAL SCIENCE. 5 (5) pp: 1810-1819. DOI: 10.1039/c3sc53088d

Rationalising the role of solid-acid sites in the design of versatile single-site heterogeneous catalysts for targeted acid-catalysed transformations

Enrica Gianotti[a], Maela Manzoli[b], Vasudev N. Shetti[c], Matthew E. Potter[d], Danni Sun[d], James Paterson[d], Alan Levy[e] and Robert Raja[d]

[a]*Dipartimento di Scienze e Innovazione Tecnologica, Centro Interdisciplinare Nano-SiSTeMI, Università del Piemonte Orientale, via T. Michel 11, I-15100, Alessandria, Italy.*
[b]*Dipartimento di Chimica e NIS-Centro di Eccellenza, Universita' di Torino, V. P. Giuria 7 – 10125 Torino, Italy.*
[c]*Refinery R&D, Reliance Industries Ltd. Jamnagar, 361142, Gujarat, India.*
[d]*School of Chemistry, University of Southampton, Highfield, Southampton SO171BJ, UK.*
[e]*Honeywell LLC, 101 Columbia Road, Morristown, NJ 07962, USA.*

Abstract

A versatile design strategy for rationalising the role of well-defined and isolated multifunctional solid-acid active centres, employing bimetallic Mg(II)Si(IV)AlPO-5 nanoporous architectures has been demonstrated, with a view to affording structure-property correlations compared to its corresponding monometallic analogues (Mg(II)AlPO-5 and Si(IV)AlPO-5). The simultaneous incorporation of Mg(II) and Si(IV) ions, as isomorphous replacements for Al(III) and P(V) ions in the microporous architecture, plays an important role in modulating the nature and strength of the solid-acid active sites in the industrially-important, vapour-phase Beckmann rearrangement of cyclohexanone oxime to produce ε-caprolactam (the precursor for renewable nylon-6) and in the isopropylation of benzene to cumene. The structural integrity, coordination geometry and local environment of the active (Brönsted-acid) sites could be rationalized at the molecular level, using *in situ* spectroscopic techniques, for tailoring the catalytic synergy by adroit design of the framework architecture.

Introduction

Engineering multifunctional active sites in nanoporous solids is an intriguing area of research that exploits the fundamental principles of solid-state chemistry. Aluminophosphates (AlPOs) are a class of nanomaterials, where single-site catalytic entities can be judiciously designed, to create novel nano-architectures.[1] In fact, isolated active centres (discrete single-sites) in AlPOs can be meticulously engineered via the isomorphous substitution of metal-ions into the alternating AlO_4 and PO_4 framework tetrahedra during synthesis.[2] By adopting this method it is possible to generate a diverse range of active sites (solid-acid and/or redox centres) within the microporous AlPO framework. In particular, tailored Brönsted acid centres can be designed in AlPOs, wherein a charge-compensating proton can instigate the accommodation of small quantities of divalent transition-metal-ions, such as Mg(II), Zn(II), etc., as isomorphous replacements for the trivalent framework Al(III) ions; or by analogously introducing tetravalent Si(IV) ions to isomorphously substitute the P(V) ions in the neighbouring PO_4 tetrahedra. Through this design strategy, it is also possible to expediently bestow multi-functionality within the *same* catalyst, through the concomitant introduction of redox-active and Brönsted acid centres, adroitly creating a bifunctional catalyst, for the 'one-pot' synthesis of ε-caprolactam directly from cyclohexanone.[3-8] More recently, we have demonstrated the ability to engineer synergistic interactions between specific metal-sites by designing redox-active centres in close proximity to oxophilic entities (e.g. $V^{V}Ti^{IV}$AlPO-5 and $Co^{III}Ti^{IV}$AlPO-5),[9,10] thereby creating functional bimetallic solid catalysts for enhancing the activity and selectivity in acid-catalysed and redox processes.[9-11]

Owing to the availability of a large-range of metal dopants that could be effectively incorporated (using the above strategies)[3,4,9-11] into a diverse-range of nanoporous architectures containing wide-range of pore apertures, it is possible to adroitly amalgamate a specific active site, with an appropriate framework, to yield a targeted catalyst capable of efficiently catalysing the industrially-important, acid-catalysed Beckmann rearrangement of cyclohexanone oxime to ε-caprolactam. ε-caprolactam is a vital commodity for the bulk chemical industry, with production exceeding 4 million metric tons per annum,[12] the vast majority of which is used as a precursor for the production of Nylon-6. In the polymer and fibre industry, Nylon-6 is generated from the *reversible* ring-opening polymerization of the monomer, ε-caprolactam; whereas Nylon-6,6 is formed by the *irreversible* dehydration polymerization of adipic acid and hexamethylene diamine.[12,13] Notwithstanding the minor physical attributes in terms of the durability and stability of these

polymers, the use of the monomer, ε-caprolactam, in the synthesis of Nylon-6, facilities the effective recovery and recycle[15] of carpet and other fibres that are derived from Nylon-6, in stark contrast to Nylon-6,6, which predominantly ends up in landfill sites.

Despite the environmentally conscious age fuelling a demand for cleaner technologies, the industrial production of the ε-caprolactam poses a number of challenges to the environment[5,14,15] and there is adequate scope for research tailored at mitigating some of these effects. Classically, ε-caprolactam is exclusively produced through the modified Raschig process (Scheme 1); a method which utilises hydroxylamine sulphate and stoichiometric quantities of oleum, to yield ε-caprolactam from cyclohexanone via a cyclohexanone oxime intermediate. Whilst the chemical yields and selectivities are noteworthy,[15] the overall atom efficiencies (and E-factor) are much inferior, as 4.4 tons of ammonium sulphate waste is generated for every ton of ε-caprolactam produced. Industrial methods that mitigate the production of ammonium sulphate to 2.6 and 1.6 tons have been reported,[16,17] but a more fundamental understanding of the precise nature of the active sites at the molecular level and its associated mechanistic implications will be required for modulating the intrinsic activity and selectivity, using benign reagents under energy-efficient conditions.[6-8,18]

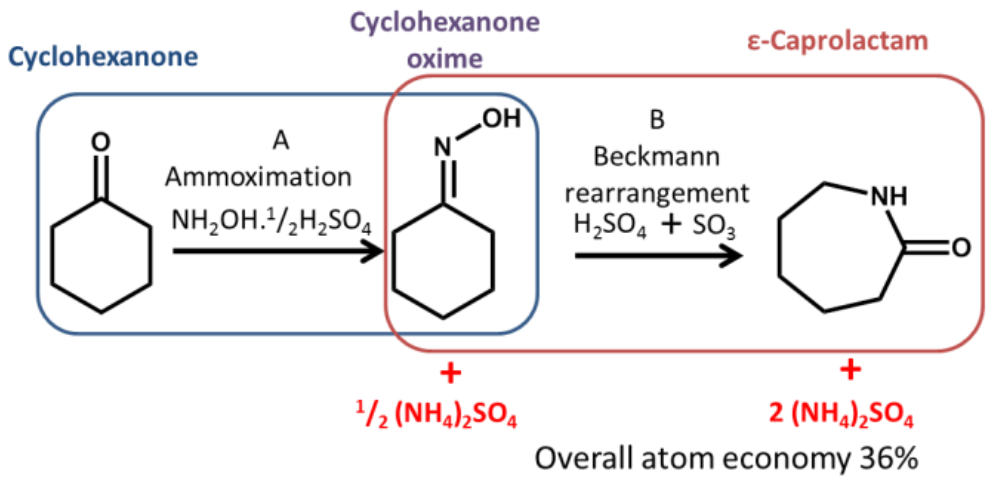

Scheme 1 Classical Raschig process

The use of heterogeneous solid-acid catalysts for the vapour-phase Beckmann rearrangement of cyclohexanone oxime is a highly desirable alternative, as it generates minimal waste and utilises benign reagents.[19,20] Furthermore, the heterogeneous nature of the solid-acid catalysts is an added advantage from the view point of costly separations associated with the Raschig method, and

circumvents the need for the neutralisation step in the work-up process. In light of this, a wide-range of materials such as TiO_2,[21] B_2O_3,[22] Nb oxides,[19] tungsten oxides[23] and rare earth pyrophosphates[24] have been reported as effective catalysts for this important transformation. In particular, the use of porous zeolitic materials has been prolific, as the combination of the crystalline structure and defect silanol groups render these materials as highly active catalysts for this process.[25-28]

The attractive features of zeotypes[29] and related mesoporous solids[30] stimulated a great deal of research into understanding the nature of the active site,[31] the role of organic solvents,[32] the importance of particular framework types,[33-36] influence of metal dopants[37] and diffusion properties linked to deactivation and lifetime of the catalyst.[38] These fundamental studies have led to the development and establishment of an industrial process that utilises a high silica MFI catalyst[34] for the commercial production of ε- caprolactam.

Despite being structurally similar, transition-metal-substituted AlPOs have not been thoroughly investigated for this reaction (part B, Scheme 1); with a majority of reports in the literature, to the best of our knowledge, confined to the use of silicon substituted AlPOs (SAPOs).[29,39] Unlike zeolites, our recent studies[9,10,20,40] have indicated that the location, proximity and nature of catalytically active centers in AlPOs can be rationally designed and judiciously controlled, in stark contrast to those of related zeolites, where post-synthetic modification methods lead to the creation of surface defects, that are the loci of the intrinsic active sites.[31] Earlier studies have indicated that strong Brönsted acid sites in zeolites play a crucial role in catalyzing the Beckmann rearrangement, by protonating the oxime.[15,41-43] However, parallel studies[44] have indicated that the presence of these strong-acid sites favor the formation of by-products, thereby decreasing the overall yield of ε-caprolactam.[45] In more recent studies, it has been suggested that weaker Brönsted acid sites and silanol groups or silanol nests play a pivotal role in modulating the selectivity in the Beckmann rearrangement of cyclohexanone oxime.[33,46]

The degree of synthetic control afforded by AlPOs for introducing a diverse range of strong and weak Brönsted acid centers is therefore highly beneficial for gaining a deeper mechanistic insight into solid-acid catalysed transformations. The complementary catalytic tests that have been outlined in this study (e.g. the Beckmann rearrangement of cyclohexanone oxime and isopropylation of benzene) along with the detailed spectroscopic measurements with appropriate molecular probes

have helped to discriminate the nature and strength of solid-acid sites required for a particular catalytic transformation.

In the present study, monometallic and bimetallic Mg- and Si-containing AlPO-5 molecular sieves (MgAlPO-5, SiAlPO-5 and MgSiAlPO-5) have been devised and used as solid-acid catalysts in the vapour-phase Beckmann rearrangement of cyclohexanone oxime to produce ε-caprolactam and in the isopropylation of benzene to form cumene. Moreover, we detail how the creation of isolated active (acid) sites, through the dual (simultaneous) incorporation of Mg^{2+} and Si^{4+} metal ions, can trigger synergistic interactions within the AlPO-5 framework architecture (see Figure 1), to enhance the catalytic activity and selectivity for the transformations shown in Figure 1.

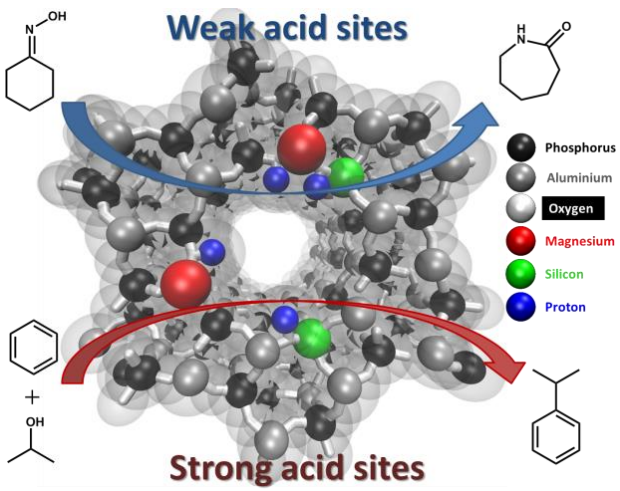

Fig 1. Pictorial representation of bimetallic MgSiAlPO-5 showing the differing influences of the active sites.

The above metals were specifically chosen due to the relative ease with which they could be isomorphoulsy incorporated into AlPO framework, to generate a diverse range of Brönsted acid sites. However, it is believed that the subtle differences in the degree of acidity typically achieved on incorporation, during synthesis, and the contrasting substitution mechanisms (Mg(II) undergoes type I substitution replacing Al(III), whereas Si(IV) undergoes type II and III substitutions to replace P(V), see Figure S1) will modulate the nature and strength of the ensuing solid-acid sites, provoking differences in catalytic behaviour. This combined with concomitant use of FTIR spectroscopy, employing both strong and weak molecular probes (2,6-dimethylpyridine and CO),

further amplifies the intrinsic synergistic interactions at the molecular level, facilitating structure-property correlations to be established.

Results and discussions

Structural and textural properties of the AlPO-5 catalysts

In order to confirm the phase-purity of the AlPO-5 architecture, a meticulous X-ray diffraction (XRD) analysis was performed on the calcined catalysts (Figure 2). It was noted that both in the monometallic and bimetallic catalysts, all the observable peaks in the XRD pattern could be attributed to the AFI framework type, suggesting no significant secondary phases or metal aggregates were present either in the fresh or post-catalysis samples (Figure S2). It was also noteworthy that the XRD results for the isomorphously-substituted analogues were in good agreement with that of the undoped AlPO-5 catalyst.

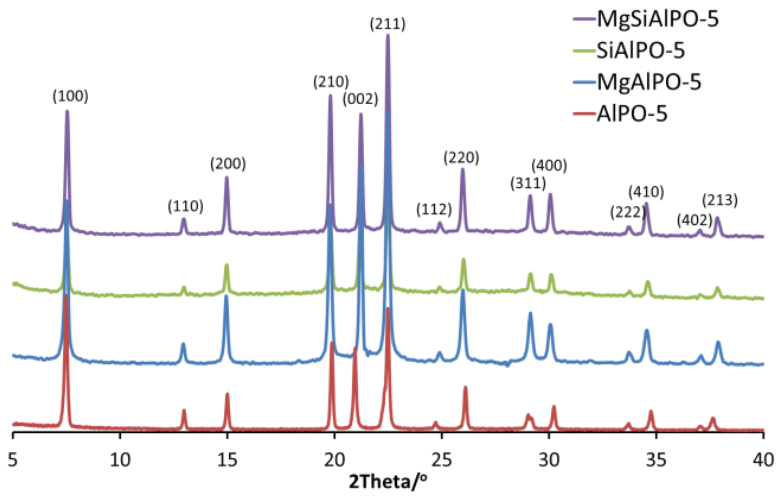

Fig. 2. Powder X-Ray diffraction patterns for calcined Mg(II)Si(IV)AlPO-5, Si(IV)AlPO-5, Mg(II)AlPO-5 and undoped AlPO-5.

Rietveld analysis (Table 1) further supports the structurally consistency between the samples; confirming that the unit cell parameters of all four catalysts are within permitted levels of experimental deviation.[47] These observations are fairly consistent, given the relatively low level of metal incorporation in the metal-substituted systems, as revealed by ICP analysis (see Table 1 and Table S2). In addition, the particle size of the samples has been evaluated (Table 1) by applying the Scherrer's equation to the (100) XRD peak, which reveals that the particle size for all four catalysts

falls within a narrow 4 nm range. Volumetric analyses confirmed the porous nature of the materials (Table 1; see also Figures S3-S8 and Table S3): the specific surface areas of the calcined metal-substituted catalysts are in good agreement with values reported in the literature for analogous systems.[48] Scanning electron microscopy (SEM) reveals spherical particles (see Figures S9-S11), with typical particle diameters ranging between 10 and 35 µm.

Table 1: Metal composition (ICP), BET surface area, particle size and unit cell parameters of the calcined AlPO-5 catalysts.

Samples	Mg wt%	Si wt%	SSA m^2g^{-1}	Particle size/nm	a/Å	c/Å
AlPO-5	-	-	295	56.5	13.69	8.43
MgAlPO-5	0.85	-	193	55.5	13.71	8.40
SiAlPO-5	-	1.69	182	54.8	13.70	8.39
MgSiAlPO-5	0.89	1.70	168	52.6	13.68	8.39

In situ vibrational FTIR spectroscopy with molecular probes for investigating the nature of active (acid) sites

FTIR spectroscopy was used to probe the nature of the acid sites by carefully examining the O-H stretching region in the microporous AlPO-5 catalysts, as shown in Figure 3. All four catalysts display a band at 3680 cm^{-1}, which is assigned to the O-H stretching mode of free P-OH defects.[49] In addition, a pronounced band at 3745 cm^{-1} is observed exclusively in the Si-containing catalysts, which is attributed to the presence of available Si-OH groups. This band is particularly distinct in the MgSiAlPO-5 catalyst, indicating the availability of a higher fraction of these sites, despite the fact that the Si-loadings are analogous when compared with the monometallic SiAlPO-5 catalyst (Table 1).

Due to the high scattering profile of the AlPO-5 catalysts in the characteristic Brönsted acid site region (typically 3600-3500 cm^{-1} in the IR spectrum), the use of probe molecules is necessary in order to gain a more detailed understanding of the Brönsted acid sites present in metal-substituted AlPO-5 catalysts. In addition, it has to be noted that, in the Si-substituted AlPO-5 catalysts, the band due to Si-OH groups (3745 cm^{-1}) is prominently discernible; indicating that the isomorphous

incorporation of Si, during synthesis, generates defects in the AFI framework. Hence in this study, a weak base (typically CO) and a strong base such as and 2,6-dimethylpiridine (2,6-DMP) were employed as a contrasting probe molecules, in order to qualitatively elucidate the acidity of the OH groups present in the AlPO-5 catalysts.

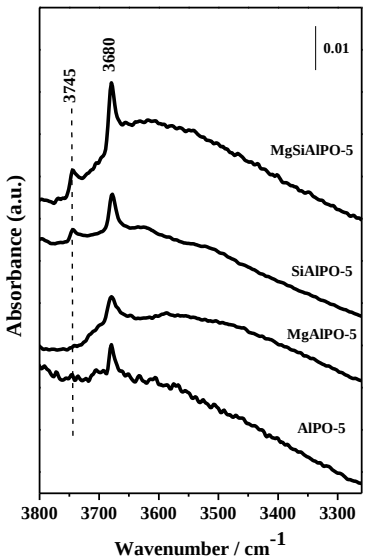

Fig. 3. FTIR spectra highlighting the OH stretching region of the Mg-, Si-, and MgSiAlPO-5. Un-doped AlPO-5 is also shown for comparison.

CO was adsorbed at 80 K on all four nanoporous catalysts, in order to specifically observe and decipher its interaction with the OH groups (Figure 4). (Note that CO is only able to interact, via H-bonding with hydroxyl groups, at low temperatures). The hydrogen-bonded C-O stretching mode emerges in the 2155-2175 cm^{-1} range, whereas the peak at 2138 cm^{-1} is attributed to liquid-like CO,[50] with the latter being particularly pronounced on adsorption of 5 mbar of CO. The spectrum of undoped AlPO-5 exhibits a band at 2165 cm^{-1}, which increases with increased CO pressure (red curve); and in conjunction with the band at 2138 cm^{-1} that has been previously attributed to liquid-like CO. The band at 2165 cm^{-1} is assigned to CO interacting exclusively with P-OH groups,[51] as these are the only hydroxyl groups present in the undoped AlPO-5 catalyst. In the spectra of the Si-containing analogues, the band at 2165 cm^{-1} displays a shoulder (particularly visible upon adsorption of 5 mbar of CO) at *ca*. 2156 cm^{-1}, which can be associated with the interaction of CO with the pendant surface silanol groups[52] present on these catalysts. The metal-substituted AlPO-5 catalysts reveal a further component at 2171 cm^{-1}, which can be assigned to the stretching mode of

the CO, interacting via H-bonding, with the more acidic hydroxyl groups that can be attributed to the Si-OH-Al or the Mg-OH-P Brönsted acid centres.[53-56] It is indeed noteworthy that the feature at 2171 cm^{-1} provides strong evidence for framework incorporation of the Mg^{2+} and Si^{4+} ions into the AlPO-5 architecture, as is evidenced from the creation of its associated Brönsted acid site (Figure 4). As such, through the use of CO as a molecular probe, it was possible to identify three separate hydroxyl groups, which due to the high scattering profile of the AlPO-5 catalysts were not visible in the O-H stretching region (c.f. Figure 3). Nevertheless, it should be pointed out that CO is unable to discriminate between Brönsted sites of different acid strengths (see later).

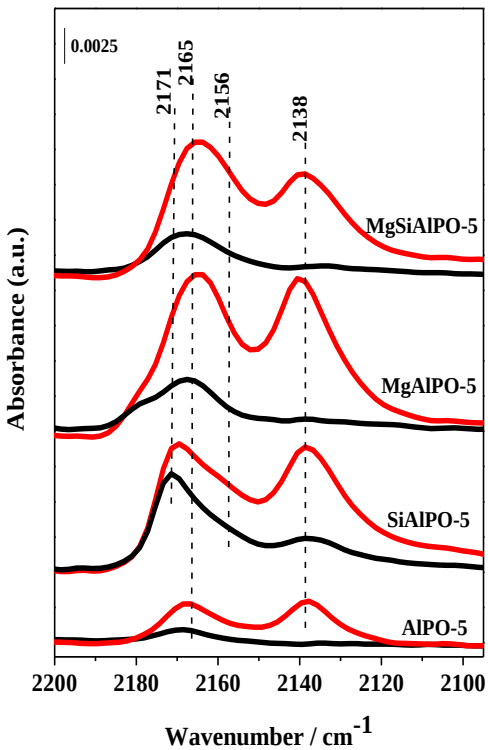

Fig. 4. FTIR spectra of CO adsorbed at 80K on mono- and bimetallic AlPO-5 catalysts; black curve: 1 mbar, red curve: 5 mbar of CO.

In order to further elucidate the nature and the strength of the Brönsted acid sites, a stronger base such as 2,6- DMP is required. Compared to pyridine, 2,6-DMP yields the protonated species more readily, due to its stronger basicity[57,58] and its weaker affinity for Lewis acid sites, owing to the steric hindrance induced by the methyl groups.[59] In Scheme 2, the IR active modes of liquid and adsorbed 2,6-DMP are highlighted. In particular, the ν_{8a} mode, which in the liquid-phase appears at 1594 cm^{-1}, is very sensitive and allows the identification of different types of 2,6-DMP adsorption

on solid catalysts. It is also striking that when the ν_{8a} wavenumber is higher than 1625 cm^{-1}, it characterises the presence of protonated species (2,6-$DMPH^+$), whereas lower wavenumber correspond to coordinated or H-bonded species (DMPL).

In Figure 5A, the FTIR spectra collected after adsorption of 2,6-DMP at 4 mbar at different contact times on the nanoporous AlPO-5 catalysts are presented. At the shorter contact times (2 minutes; black curves), bands at 1595 and 1582 cm^{-1}, due to the ν_{8a} and ν_{8b} of liquid-like 2,6-DMP are visible, together with complex bands in the 1650-1600 cm^{-1} range, assigned to the ν_{8a} and ν_{8b} modes of coordinated, protonated and H-bonded 2,6-DMP species (as shown in Scheme 2).

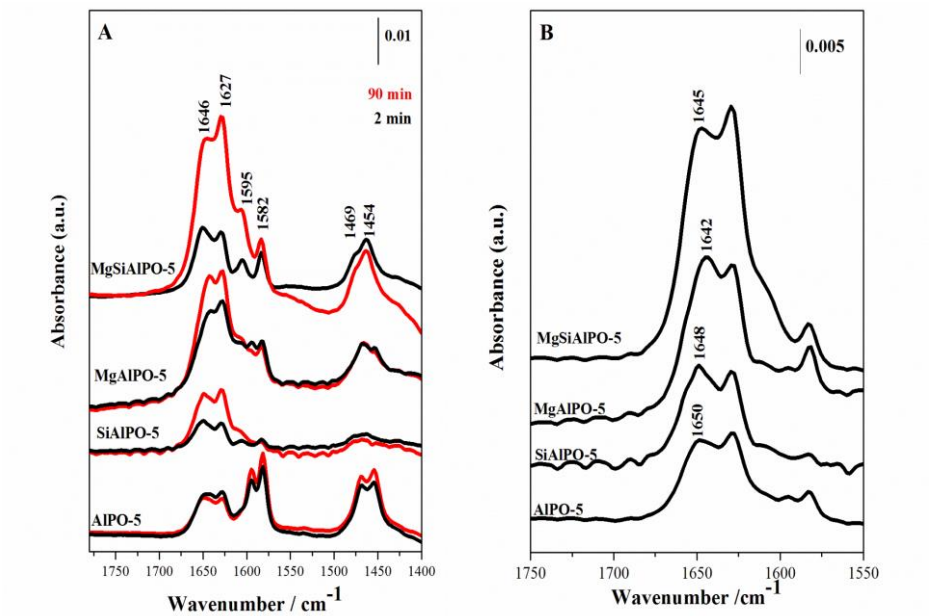

Fig.5. A) FTIR spectra of 2,6-DMP (4 mbar) adsorbed at 298K on mono- and bimetallic AlPO-5 catalysts; black curve: 2 min contact, red curve: 90 min contact. B) Corresponding FTIR spectra of outgassed 2,6-DMP at 298K on mono- and bimetallic AlPO-5 catalysts.

Bands in the 1500-1450 cm^{-1} range are also present: these are due to the ν_{19a} and ν_{19b} modes (as illustrated in Scheme 2) and can also be attributed to the bending modes of the $–CH_3$ groups. It should however be noted that the peaks in this region (1500-1450 cm^{-1}) are quite insensitive to the different coordination environments and yield very little in terms of valuable information pertaining to the nature of acid sites present in our catalysts. After prolonged contact times (90 minutes; red curves), the bands in the 1650-1600 cm^{-1} range increase in intensity and the bands due to the liquid-like molecule decrease. In the un-doped AlPO-5 catalyst, in which only P-OH groups are present

(as evidenced earlier by CO adsorption studies; Figure 4), the bands in the 1650-1600 cm^{-1} range can be assigned to 2,6-DMP, interacting via H-bonding, with the P-OH sites that are generated immediately after short exposure (2 minutes); and as expected, do not increase after prolonged contact times.

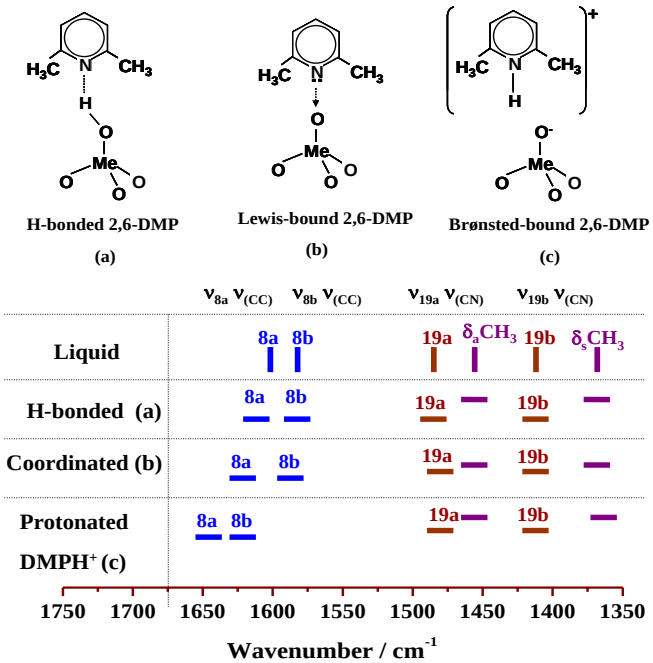

Scheme 2 IR active modes highlighting the different types of 2,6-DMP /surface interactions with the catalyst.

The ν_{8a} mode of the protonated 2,6-DMP is present in all four catalysts (1655-1640 cm^{-1} range) and, from the analysis of their relative peak positions, it is possible to deduce information on the nature and strength of the Brönsted acid sites[60]: the stronger the Brönsted acidity, the lower is the position of the ν_{8a} band. With a view to clarifying further the position of this ν_{8a} band, the FTIR spectra of the catalysts, outgassed at 298 K after 2,6-DMP adsorption, have been examined (Figure 5B). It was noted that by outgassing the catalysts, the spectra shows only spectroscopic features of the irreversibly adsorbed 2,6-DMP species. In particular, it was noted that the position of the peak maxima of the ν_{8a} band was different (Table 2) in the four catalysts used in this study and this could be used to differentiate the nature and strength of their Brönsted acid sites. By combining the spectroscopic information outlined in Figure 5 and Table 2, it has been possible to contrast the relative acid strengths of the undoped, monometallic and bimetallic catalysts and categorise the degree of their Brönsted acidity in the following order: MgAlPO-5 > MgSiAlPO-5 > SiAlPO-5 > AlPO-5; with MgAlPO-5 possessing the a greater fraction of the *strong* Brönsted acid sites, whilst

the undoped and monometallic Si-analogues exhibit a greater proclivity for the *weak* Brönsted acid sites.

Table 2. IR position and integrated area (A) of the ν_{8a}(CC) band and concentration of vibrating species (N) of the mono- and bi-substituted AlPO-5 catalysts

Catalysts	ν_{8a} (CC) / cm^{-1}	A / cm^{-1}	N / $mmolg^{-1}$
AlPO-5	1650	0.35	87
SiAlPO-5	1648	0.37	92
MgSiAlPO-5	1645	0.92	230
MgAlPO-5	1642	0.74	185

Catalysis

The varying degrees of Brönsted acid strength (as outlined from this spectroscopic study so far), which have been categorised on the basis of the interaction of 2,6-DMP with Brönsted acid centres in porous solids, prompted us to investigate the catalytic potential of these materials for solid-acid catalysed transformations. Given the intrinsic nature and strength of these solid-acid sites, we devised a series of complementary catalytic tests that would precisely implicate the role of strong, weak and intermediate Brönsted acid centres, thereby facilitating structure-property correlations to be established. With a view to achieving this goal, we investigated the Beckmann rearrangement of cyclohexanone oxime and the isopropylation of benzene to cumene, employing the monometallic, bimetallic and undoped AlPO-5 catalysts.

Catalytic tests for the vapour-phase Beckmann rearrangement of cyclohexanone oxime reveal that the SiAlPO-5 and MgSiAlPO-5 catalysts were significantly superior than MgAlPO-5, over a wide-range of temperatures (Figure 6).

In order to rationalise the differences in catalytic activity observed for the mono- and bimetallic AlPO-5 catalysts, it would be prudent to consider the reaction mechanism. The reaction mechanism for the Beckmann rearrangement of cyclohexanone oxime has been extensively studied[35,45,61-63] and is outlined in scheme 3.

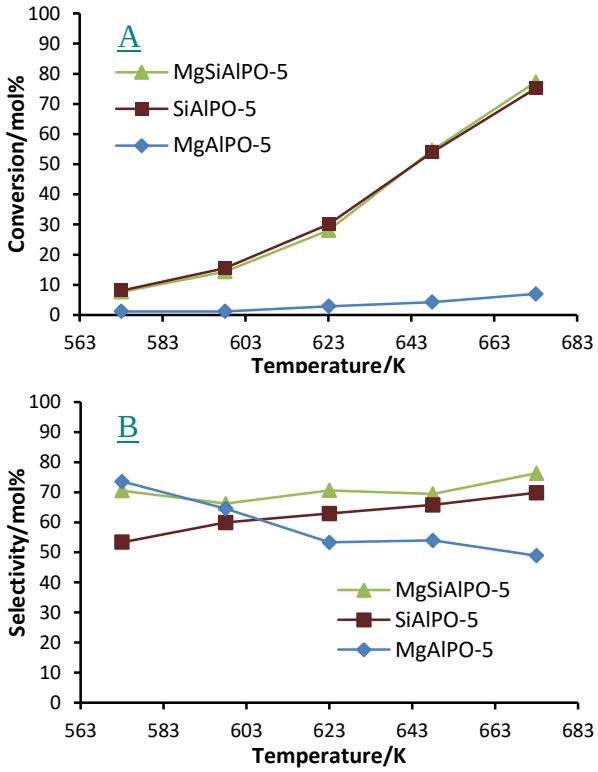

Fig. 6. Influence of temperature on the activity (A) and selectivity (B) in the Beckmann rearrangement of cyclohexanone oxime using SiAlPO-5, MgAlPO-5 and MgSiAlPO-5. Reaction conditions: Feed ≅ 300 g/l cyclohexanone oxime in methanol, catalyst = 0.25 g, WHSV = 3.3 hr^{-1}, helium flow rate = 20 ml/min.

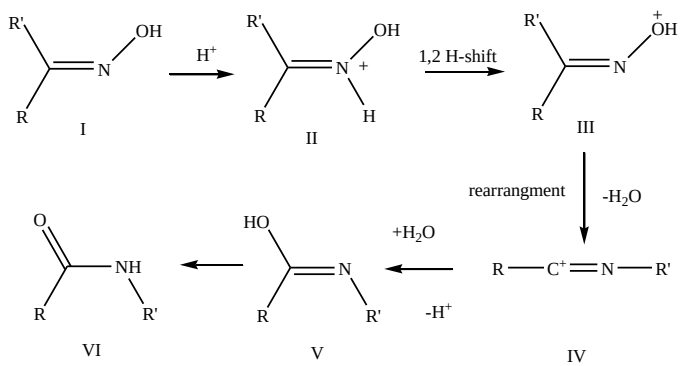

Scheme 3. Reaction mechanism for the Beckmann rearrangement of cyclohexanone oxime.

The first step is the protonation of the oxime molecule at the nitrogen atom (II); then the hydrogen is transferred from the nitrogen to the oxygen atom of the oxime (III), followed by

migration of an R group (R = alkyl, aryl or hydrogen) trans to the hydroxyl group (IV), resulting in the liberation of water. Subsequently, the displaced water hydrolyses the cation (IV) to give compound (V), which finally tautomerizes to the corresponding amide (VI). Theoretical and experimental studies[35,46,63] on the interaction of the oxime molecule with the acid sites (Brönsted sites or silanols), have shown that when only silanol groups are present, no hydrogen-atom transfer occurs from the catalyst surface and consequently the oxime is not protonated. On the other hand, when Brönsted acid sites are present, there is a complete transfer of the proton leading to the formation of the N-protonated oxime. These studies[35,46,61-63] demonstrate that the protonation of the oxime, the first step in the Beckmann rearrangement pathway, strongly depends on the acid strength of the OH groups present on the catalyst surface; and in particular, suggests that Brönsted acid sites are the most active for this step.[35,46,63] These observations strongly support the belief that the pendant silanol groups, observed during the spectroscopic FTIR characterisation, are not the active sites for this reaction; rather it is the Brönsted acid sites, resulting from the framework substitution of the heteroatoms, that initiate this reaction.

The discernible inactivity of the MgAlPO-5 catalyst further suggests that, neither the strongly acidic Mg-OH-P sites nor the weakly acidic P-OH groups observed by FTIR are the active centres for this reaction (Figure 6A). The latter of these acid sites are too weak to facilitate a reaction, whilst the former is strongly acidic and, as such, shows a greater propensity for interacting with the solvent molecules, thereby hindering any favourable interaction between the oxime and the acid site; which hinders the production of the desired ε-caprolactam.[27] This effect would be particularly pronounced within a microporous architecture, where the solvent molecules would line the pore-walls. In this scenario, the 7.3 Å cylindrical pore aperture of the AlPO-5 framework would be significantly diminished, hindering the diffusion of the bulky oxime molecule through the channels, preventing it from accessing the active sites inside the pore. It is believed that it is a combination of these factors that are responsible for the lower activity of the MgAlPO-5 catalyst.

In general it was found that the conversions increased with temperature: this behaviour can be attributed to an improved rate of diffusion of the oxime through the constrained pores and enhanced desorption of methanol with increasing temperature, resulting in a two-fold increase in the number of available active sites, which leads to the increase in catalytic efficiency. In contrast, the selectivity of the MgAlPO-5 is found to decrease with increasing temperature: this can be rationalised on the basis that the strong Brönsted acid sites facilitate the enhanced production of

side-products, which can often lead to coking and deactivation of the active site.[45,64] Furthermore, the stronger Brönsted acid sites present in MgAlPO-5 will anchor the ε-caprolactam product to the catalyst surface, and as such increasing the temperature will promote the formation of dimers, oligomers and ring-opening products through its prolonged exposure to the active site.[26]

It is observed that the MgSiAlPO-5 and SiAlPO-5 catalysts show almost an identical activity profile over a wide-range of temperatures (Figure 6A); yet, the MgSiAlPO-5 consistently demonstrates a greater specificity for the ε-caprolactam product (Figure 6B). These observations can be rationalised by considering the nature and type of hydroxyl groups present in the two catalysts. By employing *in situ* FTIR spectroscopy, it was found that both catalysts possessed a range of Brönsted acid sites, as a result of metal-incorporation, in addition to the silanol groups. As previously discussed, it is believed that it is the isolated Brönsted acid sites that are active for this reaction, and not the silanol groups. We also observed (through the adsorption of 2,6-DMP) that the Brönsted acid sites present in MgSiAlPO-5 are unique to those present in the MgAlPO-5 and SiAlPO-5 catalysts. Specifically, it was found that strength of the Brönsted acid centres present in the bimetallic catalyst is intermediary between that of the MgAlPO-5 and SiAlPO-5 catalysts.

It has been shown that in the MgAlPO-5 catalysts only strong Brönsted acid sites (Mg-OH-P) were present. Such sites appear to have a significant detrimental effect on the catalytic performance of the material, as evidenced by the significantly low conversions achieved. In the SiAlPO-5 catalyst, the silanols and Brönsted sites, Si-OH-Al, are both considerably weaker acid sites compared to Mg-OH-P, which vindicates its superior performance over that of MgAlPO-5 catalyst. In subtle contrast, the bimetallic MgSiAlPO-5 catalyst contains both types of Brönsted acid sites (Mg-OH-P and Si-OH-Al) and silanol species. The catalytic results from above (Figure 6) coupled with the findings from the FTIR spectroscopy using 2,6-DMP as a molecular probe, lead us to believe that the presence of both types of Brönsted of acid centres prompts a synergistic cooperation between the two sites, which manifests in the bimetallic catalyst possessing an acid strength that is intermediary between that of MgAlPO-5 and SiAlPO-5. This results in the bimetallic catalyst retaining an activity profile that is comparable to that of the monometallic SiAlPO-5 catalyst, though boasting a markedly superior selectivity.

Despite the MgSiAlPO-5 having a consistently higher specificity for ε-caprolactam, the selectivity of the monometallic SiAlPO-5 progressively increased with temperature. This can be attributed to thermodynamic factors, whereby the increased temperature would allow the bound 3-

caprolactam to overcome the desorption energy-barrier, thereby enhancing the desorption of 3-caprolactam from the surface of the catalyst. In doing so, this would minimise the contact time between the product and the active acid sites and hence there would be a considerably lower concentration of surface-bound 3-caprolactam to partake in by-product formation; thus lowering the rates and kinetics for the formation of higher molecular weight condensation products derived from 3-caprolactam.

The influence of WHSV (weight hourly space velocity) at 673 K (the best results were obtained at this temperature – see Figure 6) was also investigated (Figure 7 and S13), with a view to probing the influence on contact time on the activity and selectivity of the mono-substituted and bi-substituted catalysts. The increase in catalytic activity at lower WHSV can be attributed to the increased contact times of the substrate to the loci of the solid acid active centres at the expense of fewer solvent molecules that are in the vicinity, which play a detrimental role in blocking access to these active centres. We further note that by decreasing the WHSV (Figures 7A and B), significant differences start to manifest, which translates to a large (>10 mol%) difference in caprolactam yield (see Figure S13) between the SiAlPO-5 and MgSiAlPO-5 catalysts, which is quite revealing. These results further vindicate our earlier findings that, in addition to process variables, the nature and strength of the isolated, Brönsted acid active centres play a far more critical role in influencing the activity and selectivity of solid catalysts, in the Beckmann rearrangement of cyclohexanone oxime to ε-caprolactam.

Given the diverse array of strong, intermediate and weak Brönsted acid centres that are present in our monometallic and bimetallic catalysts, we devised a complementary catalytic test, which has been well-established in the literature,[65-67] to involve strong Brönsted acid centres. The isopropylation of benzene to cumene is catalysed by strong Brönsted acid centres[65-67] and MgAlPO-5 is known to be highly active for this reaction.[68] The high activity of this catalyst has been attributed to the fact that the framework incorporation of magnesium is known to produce one of the strongest Brönsted acid sites within an AlPO architecture.[69] We observed that our MgAlPO-5, which was fairly inactive for the Beckmann rearrangement of cyclohexanone oxime, was reasonably active and selective (Figure 8) for the isopropylation of benzene, justifying our rationale from the FTIR spectroscopic observations, that this catalyst contains an overwhelming majority of strong Brönsted acid active centres.[20] Consistent with the above arguments, it was noted that the SiAlPO-5 catalyst, which contains a higher proportion of weak acid sites, displays an inferior

catalytic performance (Figure 8), when compared with the MgAlPO-5. It was, however, rather surprising that the bimetallic MgSiAlPO-5 again demonstrates a much higher catalytic activity, particularly when compared to MgAlPO-5.

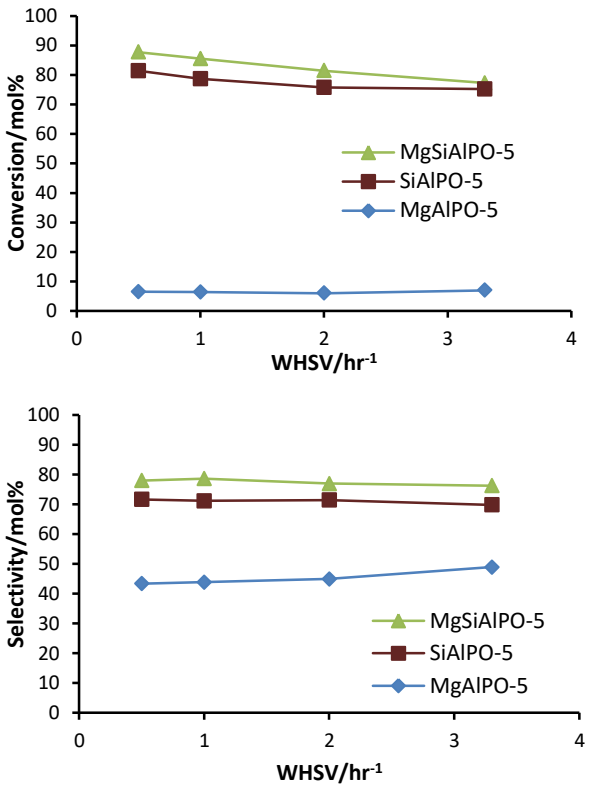

Fig. 7. Influence of WHSV on activity (A) and selectivity (B) in the Beckmann rearrangement of cyclohexanone oxime using Mg and Si containing monometallic and bimetallic catalysts. Reaction conditions: Feed ≅ 300 g/l cyclohexanone oxime in methanol, catalyst = 0.25 g, WHSV = 3.3 hr^{-1}; T = 673 K, helium flow rate = 20 ml/min.

Given the nature of the acid sites and on the basis of the relative acid strengths (as summarised in Table 2), it was to be expected that MgAlPO-5, containing an overwhelming majority of strong Brönsted acid sites, was more active than the SiAlPO-5 analogue. Contrary to expectations, the bimetallic MgSiAlPO-5, that possesses intermediate strength Brönsted acid centres, displays superior catalytic properties when compared to its monometallic counterparts. In line with our earlier observations, this synergistic enhancement in catalytic activity can be attributed to the presence of both the Mg(II) and Si(IV) ions, the loci of the Mg-OH-P and Si-OH-Al Brönsted acid

centres, within the same AlPO framework, and this can be further substantiated by considering the reaction mechanism.

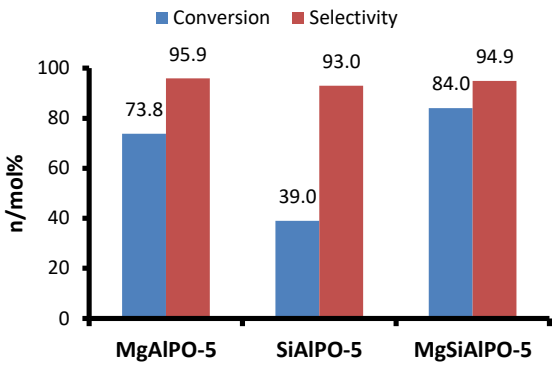

Fig. 8. Catalytic results for the isopropylation of benzene with isopropanol using Mg and Si containing monometallic and bimetallic catalysts. Reaction conditions: WHSV = 3.3 hr^{-1}; T = 323 K; benzene:isopropanol feed ratio = 6:1 mol; He flow rate ≅ 10ml/min.

The isopropylation reaction is known[65-67] to proceed via a multi-step pathway, comprising of the dehydration of the 2-propanol and subsequent alkylation of benzene. An efficient catalyst should therefore comprise of the requisite active centres that are able to successfully catalyse these individual steps. It has recently emerged[11,70] that Si-containing zeolites and related zeotypes are efficient catalysts for the dehydration of alcohols and we believe that the Si-OH-Al Brönsted acid centres in the bimetallic catalyst trigger the dehydration of 2-propanol. The subsequent protonation of the olefin requires strong Brönsted acid centres and the ready availability of the Mg-OH-P sites, in close proximity to the Si-OH-Al centres, we believe, is critical for the enhanced performance observed with the bimetallic MgSiAlPO-5 catalyst. The overall effectiveness in catalysing these tandem reactions is fundamental to the rate-determining step, that involves the electrophilic attack of the protonated olefin and benzene.

Conclusions

A resourceful strategy for the design and creation of a novel bimetallic heterogeneous catalyst has been developed, wherein a unique array of multifunctional solid-acid Brönsted acid centres (comprising of Mg-OH-P and Si-OH-Al) and silanol species have been introduced through

simultaneous isomorphous substitution of the AlO_4 and PO_4 framework tetrahedra. The precise location, geometry, nature and strength of these active centres has been probed and characterised using a combination of structural, physico-chemical, and *in situ* spectroscopic techniques using molecular probes, with a view to affording structure-property correlations, in two contrasting acid-catalysed transformations that require distinct Brönsted acid centres. In particular, synergistic enhancements in catalytic behaviour have been observed with the MgSiAlPO-5 catalyst in the industrially significant Beckmann rearrangement of cyclohexanone oxime to ε-caprolactam and in the isopropylation of benzene to cumene. These findings have been rationalised in terms of the loci of the active sites and their specific role in tailoring the Brönsted acid strength for influencing the desired reaction pathway, from a mechanistic perspective, at the molecular level. By gaining a thorough understanding of the precise nature and strength of the solid-acid active centres, it has been possible to predict the type of substitution mechanism that leads to the creation of isolated single-sites for targeted catalysis. We believe that this represents the genesis of predictively designing multifunctional sites for enhancing the synergy in catalytic transformations and emphasises the importance of using a multidisciplinary approach that is allied with operando spectroscopy.

Acknowledgment

We wish to thank the British-Italian partnership program for funding this research. MEP is grateful to Honeywell Int. for a PhD scholarship, and we are grateful to Compagnia di San Paolo for sponsorship to NIS – Centre of Excellence (Torino). We are also grateful to Cambridge Reactor Design (CRD) for their invaluable help in reactor design and configuration. We would also like to acknowledge Marvin Shachter and Nancy Darko of UOP for their assistance in performing NH_3-TPD and BET analysis respectively.

Notes and references

1 M. Hartmann and L. Kevan, *Chem. Rev*., 1999, **99**, 635-664.

2 L. Gómez-Hortigüela, F. Corà, G. Sankar, C. M. Zicovich-Wilson and C. R. A. Catlow, *Chem. Eur. J.,* 2010, **16**, 13638-13645.

3 R. Raja, G. Sankar, and J. M. Thomas, *J. Am. Chem. Soc.,* 2001, **123**, 8153-8154.

4 R. Raja and J. M. Thomas, *Proc. Natl. Acad. Sci*., 2005, **39**, 13732-13736.

5 R. Moyaka and M. Poliakoff, *Nature,* 2005, **437**, 1243-1244.

6 R. Raja, US2010/0179317 A1.

7 R. Raja and J. M. Thomas, US Patent 2013/0245323.

8 R. Raja and A. J. Paterson, US Patent 2013/0245322.

9 J. Paterson, M. E. Potter, E. Gianotti and R. Raja, *Chem Commun.,* 2011, **47**, 517-519.

10 R. M. Letihall, V. N. Shetti, S. Maurelli, M. Chiesa, E. Gianotti and R. Raja, *J. Am. Chem. Soc*., 2013, **135**, 2915-2918.

11 M. Lefenfeld, R. Raja, A. J. Paterson and M. E. Potter, US Patent 021882, 2010.

13 Product focus, Chem. Week 7, 2007.

12 I. M. Kohan, In Nylon Plastics Handbook; Hanser/Gardner: New York, 1995, Chapter 13, p 519.

14 G. Bellussi and C, Perego, *CATTECH*, 2000, **4**, 4-16.

15 G. Dahlhoff, J. P. M. Niederer and W. F. Hoelderich, *Catal. Rev.–Sci. Eng.,* 2001, **43**, 381-441.

16 G. Petrini, G. Leofanti, M.A. Mantegazza and F. Piagnataro, *Caprolactam via Ammoximation, American Chemical Society Symp. Ser.,* American Chemical Society, Washington, 1996, **626**, 33.

17 J. Ritz, H. Fuchs, H. Kieczka and W.C. Moran, *Ullmann's Encyclopaedia of Industrial Chemistry*, Vol A5, VCH Verlagsgsellschaft mbH, Germany, 1986, 31.

18 A. Levy, R. Raja and M. E. Potter, WO2013063244 A1 and US20130109851.

19 M. Anilkumar and W.F. Hoelderich, *J. Catal.,* 2008, **260**, 17-29.

20 M. E. Potter, D. Sun, E. Gianotti, M. Manzoli and R. Raja, *Phys. Chem. Chem. Phys.*, 2013, **15**, 13288-13295.

21 H. Sharghi and M. H. Sarvari, *J. Chem. Res.,* 2003, **3**, 176-178.

22 T. Curtin, J. B. McMonagle and B. K. Hodnett, *Appl. Catal. A: Gen.,* 1992, **93**, 91-101.

23 N. Kob and R. S. Drago, *Catal. Lett.,* 1997, **49**, 229-234.

24 Z. Zhang, J. Li and X. Yang, *Catal. Lett.,* 2007, **118**, 300-305.

25 W.F. Hoelderich, J. Roseler, G. Heitmann and A.T. Liebens, *Catal. Today,* 1997, **37**, 353-366.

26 C. Flego and L. Dalloro, *Micropor. Mesopor. Mater.*, 2003, **60**, 263-271.

27 L. X. Dai, K. Koyama, M. Miyamoto and T. Tatsumi, *Appl. Catal. A. General,* 1999, **189**, 237.

28 H. Kath, R. Glaser and J. Weitkamp, *Chem. Eng. Tech.,* 2001, **24**, 150-153.

29 P. S. Singh, R. Bandyopadhyay, S. G. Hegde and B. S. Rao, *Appl. Catal. A: Gen.*, 1996, **136**, 249-263.

30 K. Chaudhari, R. Bal, A. J. Chandwadkar and S. Sivasanker, *J. Mol. Catal. A: Chem.*, 2002, **177**, 247-253.

31 G. P. Heitmann, G. Dahlhoff, W. F. Hoelderich, *Appl. Catal. A: Gen.*, 1999, **185**, 99-108.

32 T. Komatsu, T. Maeda and T. Yashima, *Micropor. Mesopor. Mater.*, 2000, **35**, 173-180.

33 J. Sirjiaraensre, T. N. Truong and J. Limtrakul, *J. Phys. Chem. B,* 2005, **109**, 12099-12106.

34 Y. Izumi, H. Ichihashi, Y. Shimazu, M. Kitamura and H. Sato, *Bull. Chem. Soc. Jpn.*, 2007, **80**, 1280-1287.

35 A. B. Fernandez, M. Boronat, T. Blasco, and A. Corma, *Angew. Chem. Int. Ed*., 2005, **44**, 2370-2373.

36 J. Sirijaraensre and J. Limtrakul, *Chem. Phys. Chem.*, 2006, **7**, 2424-2432.

37 R. Anand, R. B. Khomane, B. S. Rao and B. D. Kulkarni, *Catal. Lett.*, 2002, **78**, 189-194.

38 A. Cesana, S. Palmery, R. Buzzoni, G. Spano, F. Rivetti and L. Carnelli, *Catal. Today,* 2010, **154**, 264-270.

39 K. D. Olson, US Patent 251168, 1988.

40 M. E. Potter, A. J. Paterson, R. Raja, *ACS Catal.*, 2012, **12**, 2446-2451.

41 H. Sato, *Catal. Rev.– Sci. Eng*., 1997, **39**, 395-424.

42 A. Aucejo, M. C. Burguet, A. Corma and V. Fornes *J. Catal.*, 1986, **22**, 187-200.

43 A. Camblor, A. Corma, H. Garcia, V. Semmer-Herledan and S. Valencia, *J. Catal.*, 1998, **177**, 267-272.

44 H. Ichihashi and M. Kitamura, *Catal. Today*, 2002, **73**, 23-28.

45 V. R. Reddy Marthala, Y. Jiang, J. Huang, W. Wang, R. Glaser and M. Hunger, *J. Am. Chem. Soc*., 2006, **128**, 14812-14813.

46 J. Sirijaraensre and J. Limtrakul, *Phys. Chem. Chem. Phys*., 2009, **11**, 578-585.

47 M. M. J. Treacey and J. B. Higgins, *Collection of simulated XRD powder patterns for Zeolites*, Elsevier Science and Technology, 5th Edition.

48 L. Zhou, J. Xu, C. Chen, F. Wang and X. Li, *J. Porous Mater.*, 2008, **15**, 7-12.

49 L. Marchese, J. Chen, J. M. Thomas, S. Coluccia and A. Zecchina, *J. Phys. Chem.*, 1994, **98**, 13350-13356.

50 G. E. Ewing, *J. Chem. Phys*., 1962, **37**, 2250-2256.

51 E. Gianotti, V. Dellarocca, E. C. Oliveira, S. Coluccia, H. O. Pastore and L. Marchese, *Stud. Surf. Sci. Catal.*, 2002**, 142**, 1419-1426.

52 E. Gianotti, C. Bisio, L. Marchese, M. Guidotti, N. Ravasio, R. Psaro and S. Coluccia *J. Phys. Chem. C,* 2007**, 111**, 5083-5089.

53 S. Bordiga, C. Lamberti, F. Geobaldo, A. Zecchina, G. Turnes Palomino and A. Zecchina, *Langmuir*, 1995, **11**, 527-533.

54 O. Cairon, T. Chevreau and J-C. Lavalley, *J. Chem. Soc. Faraday Trans.*, 1998, **94**, 3039-3047.

55 G. V. A. Martins, G. Berlier, C. Bisio, S. Coluccia, H. O. Pastore and L. Marchese, *J. Phys. Chem. C,* 2008, **112**, 7193-7200.

56 K. Chakarova and K. Hadjiivanov, *J. Phys. Chem. C*, 2011, **115**, 4806-4817.

57 C. Lahousse, A. Aboulayt, F. Mauge', J. Bachelier and J. C. Lavalley, *J. Mol. Catal.*, 1993, **84**, 283-297.

58 E. P. Hunter and S. G. Lias, *J. Phys. Chem. Ref. Data*, 1998, **27**, 413-656.

59 P. A. Jacobs and C. F. Heylen, *J. Catal.*, 1974, **34**, 267-274.

60 L.Oliviero, A. Vimont, J-C. Lavalley, F. Romero Sarria, M. Gaillard and F. Mauge', *Phys. Chem. Chem. Phys*., 2005, **7**, 1861-1809.

61 P. S. Landis and P. B. Venuto, *J. Catal.*, 1966, **6**, 245-252.

62 A. B. Fernandez, I. Lezcano-Gonzales, M. Boronat, T. Blasco and A. Corma, *J. Catal.*, 2007, **249**, 116-119.

63 I. Lezcano-Gonzales, A. Vidal-Moya, M. Boronat, T. Blasco and A. Corma, *Phys. Chem. Chem. Phys*., 2010, **12**, 6396-6403.

64 H. Ichihiashi and M. Kiamura, *Catal. Today*, 2002, **73**, 23-28.

65 S. K. Saha, S. B. Waghmode, H. Maekawa, K. Koruma, Y. Kubota, Y. Sugi, Y. Oumi and T. Sano, *Micro. Meso. Mater.*, 2005, **81**, 277-287.

66 S. Barman, *J. Appl. Sci.*, 2010, **10**, 2602-2607.

67 J. Joni, M. Haumann and P. Wasserscheid, *Appl. Catal. A: Gen.*, 2010, **372**, 8-15.

68 S. K. Saha, S. B. Waghmode, H. Maekawa, K. Komura, Y. Kubota, Y. Sugi, Y. Oumi and T. Sano, *Micropor. Mesopor. Mater.*, 2005, **81**, 289-303.

69 F. Cora, M. Alfredsson, C.M. Barker, R.G. Bell, M.D. Foster, I. Saadoune, A. Simplerer and C.R.A. Catlow, *J. Solid State Chem.*, 2003, **176**, 496-529.

70 J. N. Kondo, K. Ito, E. Yoda, F. Wakabayashi and K. Domen, *J. Phys. Chem. B*, 2005, **109**, 10969-10972.

SUPPORTING INFORMATION

Rationalising the role of solid-acid sites in the design of versatile single-site heterogeneous catalysts for targeted acid-catalysed transformations.

Enrica Gianotti[a], Maela Manzoli[b], Vasudev N. Shetti[c], Matthew E. Potter[d], Danni Sun[d], James Paterson[d], Alan Levy[e] and Robert Raja[d]

[a]Dipartimento di Scienze e Innovazione Tecnologica, Centro Interdisciplinare Nano-SiSTeMI, Università del Piemonte Orientale, via T. Michel 11, I-15100, Alessandria, Italy.

[b]Dipartimento di Chimica e NIS-Centro di Eccellenza, Universita' di Torino, V. P. Giuria 7 – 10125 Torino, Italy.

[c]Refinery R&D, Reliance Industries Ltd. Jamnagar, 361142, Gujarat, India.

[d]School of Chemistry, University of Southampton, Highfield, Southampton SO171BJ, UK. Tel: +44 (0)23 8059 2144; E-mail: R.Raja@soton.ac.uk.

[e]Honeywell LLC, 101 Columbia Road, Morristown, NJ 07962, USA.

Experimental

Synthesis

The synthetic protocol for the isomorphous substitution of Mg and Si into the AFI framework (MgSiAlPO-5) is described (below); an analogous method was employed for the preparation of the monometallic counterparts, details of which are provided in Table 1 (below). The synthesis method to form MgSiAlPO-5 involved initially adding 4.0 g of aluminium hydroxide hydrate (Aldrich) to a homogeneous solution of 5.0 g of phosphoric acid (85% in H2O, Aldrich) in 20 ml of water and allowing the mixture to stir for 10 minutes. Aqueous homogeneous solutions of 0.33 g of magnesium(II) acetate tetrahydrate (Aldrich) in 10 ml of water and 0.62 g of fumed silica (Aldrich) were added simultaneously to the above solution, which resulted in the formation of a viscous gel, which was stirred for a further 30 minutes in order to obtain a homogeneous mixture. N,N-methyldicyclohexylamine (SDA) (Aldrich) (8.0 g) was then added slowly followed by 20 ml of water with vigorous stirring for 60 minutes in order to obtain a white gel with the composition 1.0Al: 0.85P: 0.80MDCHA: 50H2O: 0.03Mg: 0.20Si.

The contents of the gel were sealed in a Teflon-lined stainless-steel autoclave, which was then transferred to a pre-heated, fan-assisted oven (WF-30 Lenton) that was set to the desired temperature of 190 ^{o}C, prior to the onset of the crystallisation. The autoclave was heated at 190 ^{o}C under autogeneous pressure for 2 hr. The white solid product was collected by filtration, washed with approx. 500 ml deionised water, and dried in air (60 ^{o}C) for 12 hours. The as-prepared sample was calcined in a tube furnace under a flow of air at 550 ^{o}C for 12 hours yielding a white solid. The synthesis procedure for other samples in this study, were analogous to the above, but with appropriate variations in the crystallisation temperature and gel composition that are shown in Table S1.

Table S1. Specific synthesis conditions for metal-substituted AlPOs.

Sample	Molar gel composition	Crystallization temp/ ^{o}C
AlPO-5	1.00P:1.00Al:0.75TEA:25H_2O	200
MgAlPO-5	1.50P:1.00Al:0.04Mg:0.80MDCHA:60H_2O	200
SiAlPO-5	0.75P:1.00Al:0.25Si:0.65MDCHA:40H_2O	200
MgSiAlPO-5	0.85P:1.00Al:0.03Mg:0.20Si:0.80MDCHA:50H_2O	190

Characterisation

X-Ray powder diffraction patterns were obtained using a Siemens D5000 diffractometer using Cu Kα1 radiation, where λ = 1.54056 Å. Scanning electron microscopy images were obtained using a JOEL-JSM5910 microscope with accelerating voltage of 0.3-30 kV. The samples were prepared by carbon coating. BET surface area measurements were performed using a Micromeritics Gemini 2375 surface area analyser and prepared using flow gas preparation. A Perkin-Elmer Optimum 3000 DV was used for ICP analyses with calcined samples prepared and fully digested in 10ml of deionised water and 10ml of ACS Plus Certified H_2SO_4 (Fisher Scientific). Solutions of standard concentrations were used for calibration. FTIR spectra of self-supporting wafers of the samples (ca. 5 mg cm^{-2}) were recorded with a Bruker IFS88 spectrometer at a resolution of 4 cm^{-1}. All samples were re-calcined at 823K in oxygen to remove the adsorbed species before the FTIR experiments. CO was adsorbed at 80K and 2,6-DMP was adsorbed at room temperature on the calcined samples, using specially designed cells which were permanently connected to a vacuum line (ultimate pressure $<10^{-5}$ Torr) to perform adsorption-desorption in situ measurements. FTIR spectra were reported in difference mode by subtracting the spectrum of the sample in vacuo to the spectrum of the adsorbed probe molecules. Multi-peak fitting was performed by employing ORIGIN 6.1 Scientific Graphics and Analysis Software. Lorentzian functions were used and a R2 =0.99714 was obtained. All TPD measurements were performed on a custom-built system using TCD detectors to monitor ammonia concentration. As-synthesised materials were pre-treated by heating at 10oC/min to 550ºC in a 20% O2/ helium mixture [Matheson UHP grade passed through a Drierite/molecular sieve gas purifier (Alltech Associates)] and held for 2 hours. The samples were exposed to ammonia and allowed to equilibrate at 150ºC for 8 hours. Desorption was performed in flowing helium [Matheson UHP grade further purified with an Oxy-Trap (Alltech Associates) and an indicating OMI-1 purifier (Supelco)] at 10oC/min to 600oC and held for 40 minutes at 600ºC.

Catalysis

Beckmann rearrangement of cyclohexanone oxime

A cylindrical quartz fixed-bed reactor (4 mm in diameter) with a quartz frit was packed with a 5 mm layer of glass beads, a 40 mm layer of pelletized catalyst (0.25 g) and a further 60 mm layer of glass beads, was placed inside the heater unit of the reactor assembly. The sample was then pretreated at 673 K under a 20 ml/min flow of helium gas for 1 hour. The temperature was then decreased to 573 K and a liquid-feed of 300 g/litre of cyclohexanone oxime in methanol was fed into the reactor, maintaining a WHSV of 3.3 hr^{-1} that was controlled by an electronic mass-flow controller, with a sample being taken after an hour, when steady-state was achieved. The temperature was then systematically increased to 598, 623, 648 and 673 K and samples were taken at each temperature after being allowed to equilibrate for an hour. The temperature was then held at 673 K while the flow-rate was systematically changed employing the mass-flow controller to give a WHSV of 2.0, 1.0 and 0.5 hr^{-1}. Samples were taken at each flow rate after being allowed to

equilibrate for one hour. Samples were analysed using a Clarus 400 gas chromatogram with FID and using an Elite 5 column, the peak areas were calibrated using pre-determined response factors.

Isopropylation of Benzene

The quartz reactor and catalyst were pre-treated as described above. The temperature was decreased to 523 K and a liquid feed of 6:1 molar ratio of benzene:isopropanol was employed with a WHSV of 3.5 hr^{-1} under a flow of 10 ml/min of helium carrier gas. Samples were taken after 1 hour of equilibration and were analysed by GC as described above.

Substitution mechanism

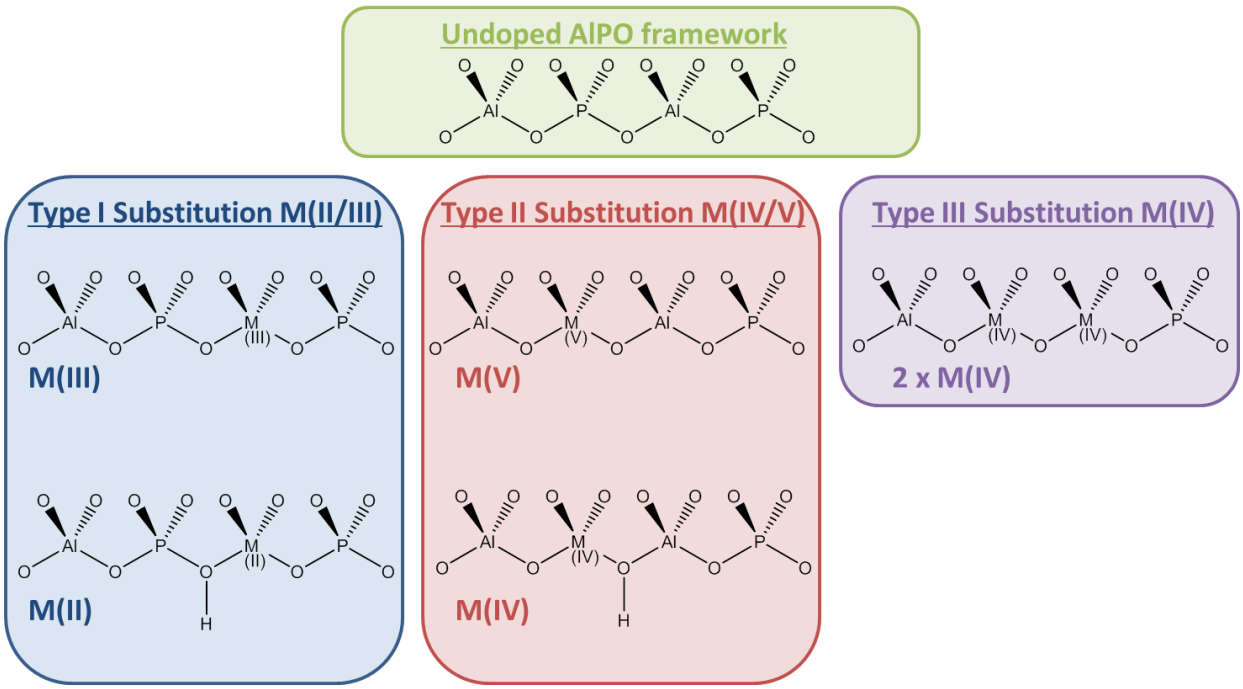

Figure S1: Scheme outlining the metal substitution mechanisms in AlPO frameworks.

Powder XRD analysis post-reaction

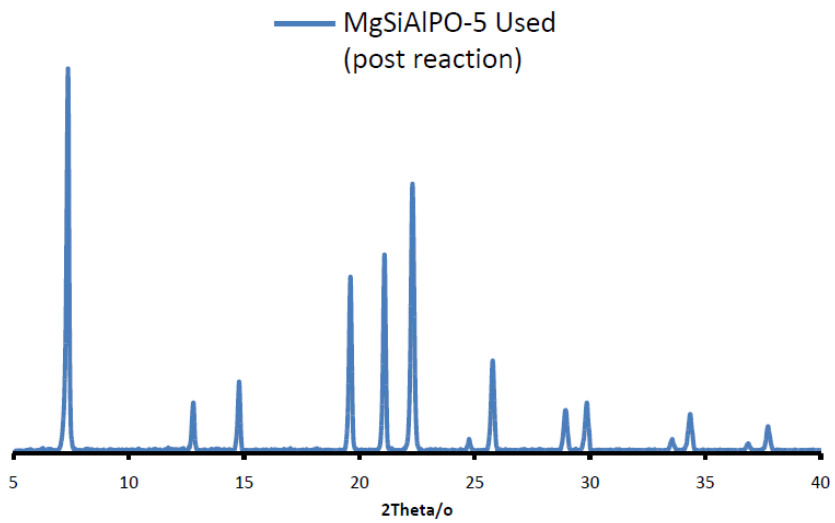

Figure S2: Powder XRD pattern of the used MgSiAlPO-5 catalyst after the Beckmann rearrangement reaction (8 hours, time-on-stream).

Full ICP results

Table S2: Full ICP results of AlPO-5 systems

Sample	Al/wt%	P/wt%	Mg/wt%	Si/wt%
AlPO-5	18.1	16.7	N/A	N/A
MgAlPO-5	15.9	20.6	0.85	N/A
SiAlPO-5	19.8	14.7	N/A	1.69
MgSiAlPO-5	18.0	14.6	0.89	1.70

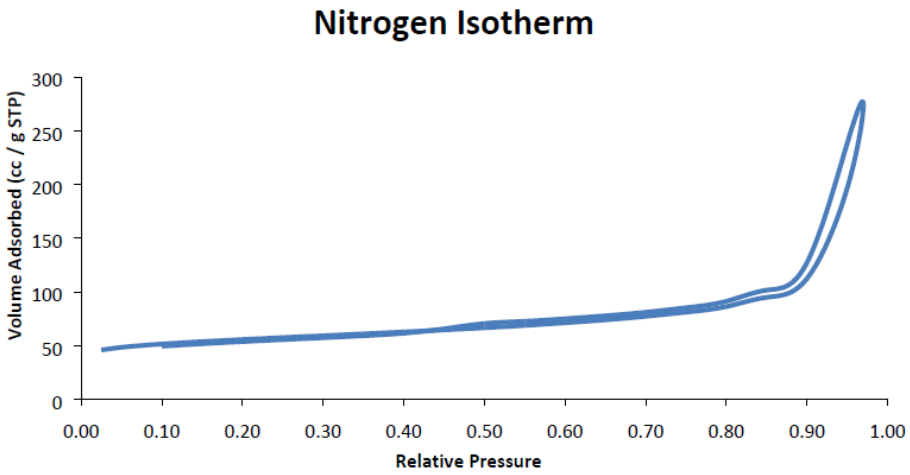

Figure S3: Nitrogen adsorption isotherm for MgSiAlPO-5.

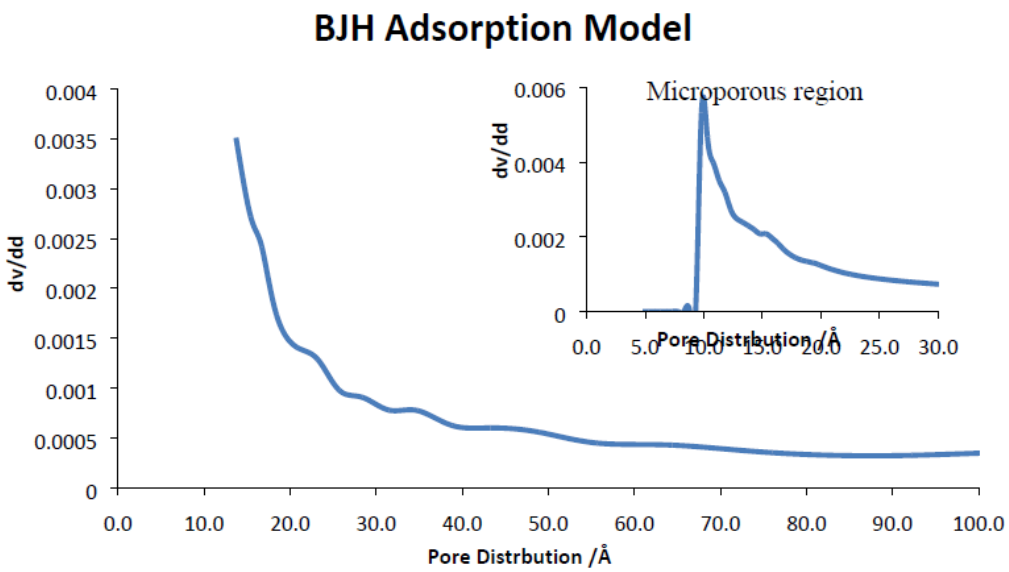

Figure S4: BJH Adsorption model plot for MgSiAlPO-5.

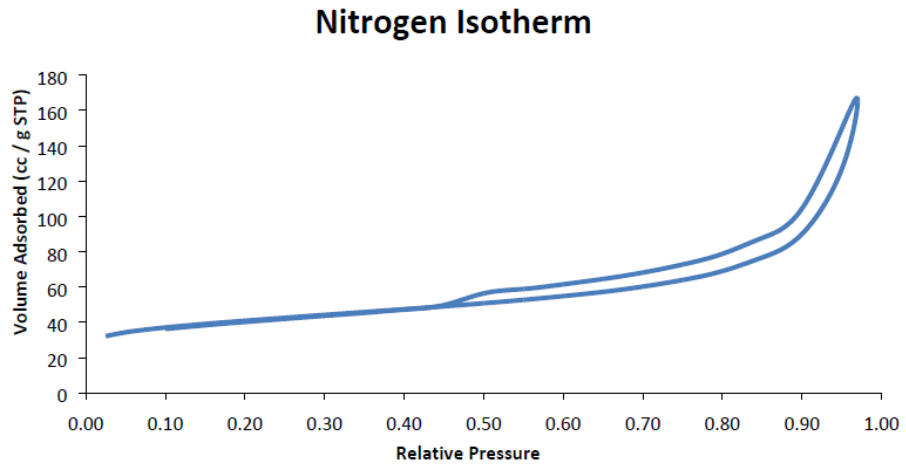

Figure S5: Nitrogen adsorption isotherm for SiAlPO-5.

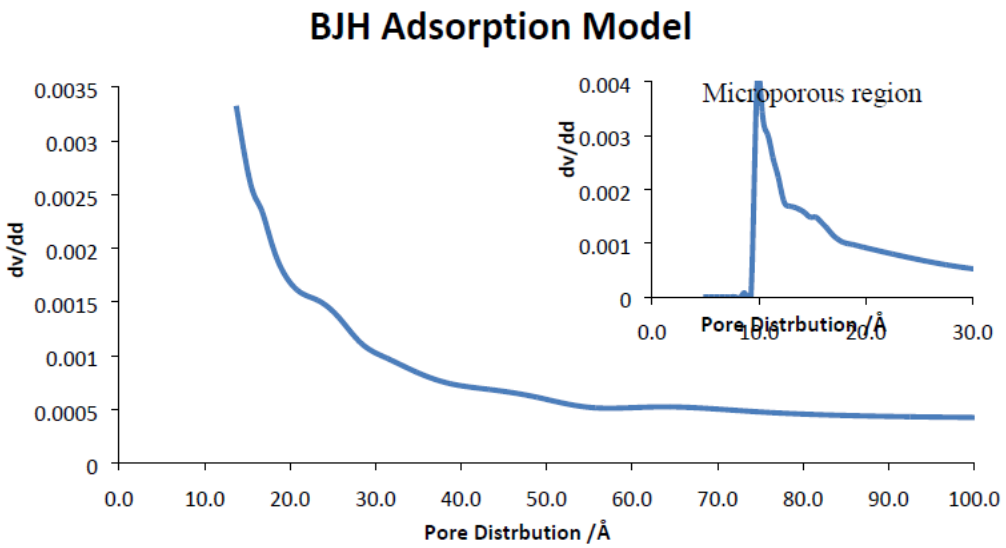

Figure S6: BJH Adsorption model plot for SiAlPO-5.

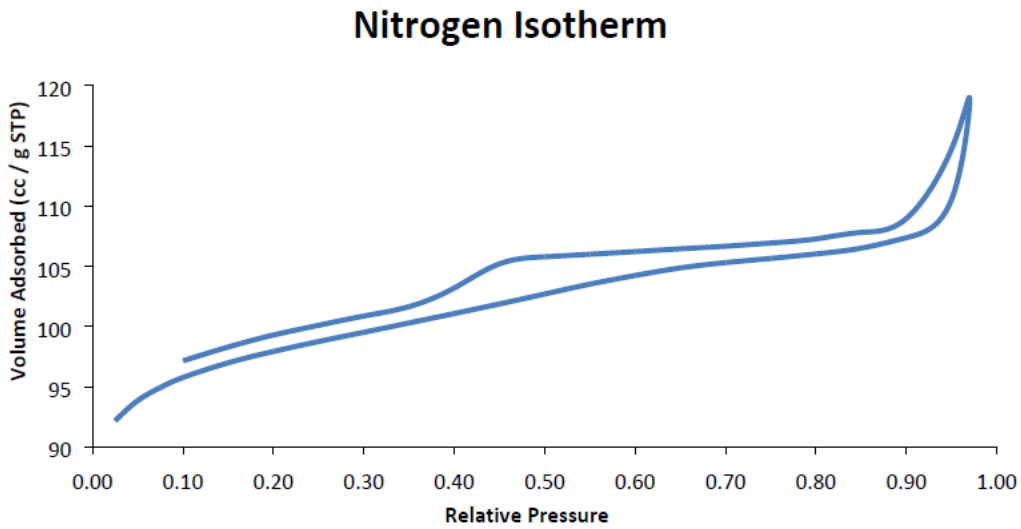

Figure S7: Nitrogen adsorption isotherm for MgAlPO-5.

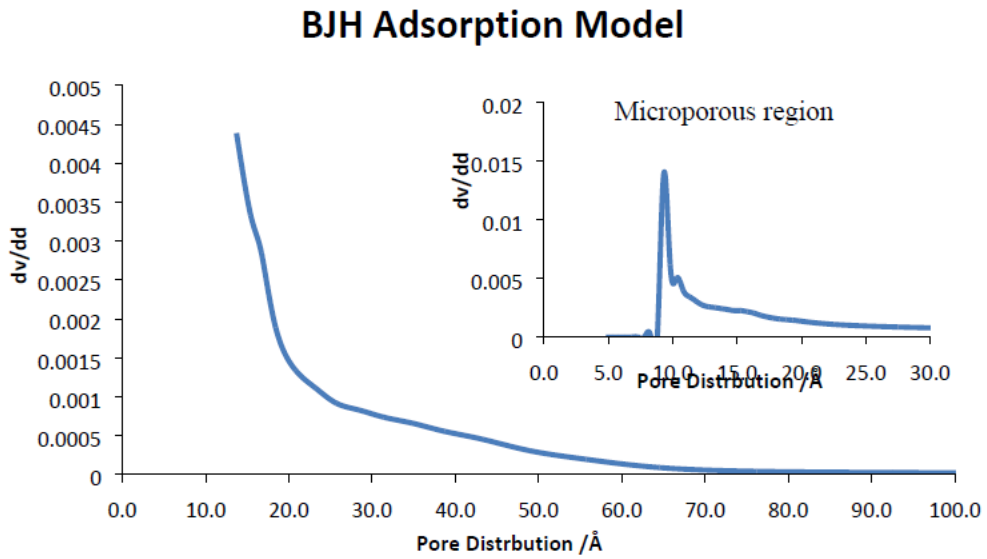

Figure S8: BJH Adsorption model plot for MgAlPO-5.

The hysteresis plots are consistent with those reported in the literature (G. C. Bond, et al, *J. Chem. Soc. Commun*., 1988, **15**, 1056-1057; L. Zhou et al., *Micropor. Mesopor. Mater.*, 2012, **161**, 76-83) for analogous AlPO-5 catalysts and the BJH model shows no significant bands in the mesoporous region, thereby confirming the microporous nature of our catalysts.

Table S3: Micropore volume from BET T-plot.

Sample	**T-plot micropore volume/(cm^3/g)**
MgSiAlPO-5	0.057760
SiAlPO-5	0.03257
MgAlPO-5	0.115138

SEM images

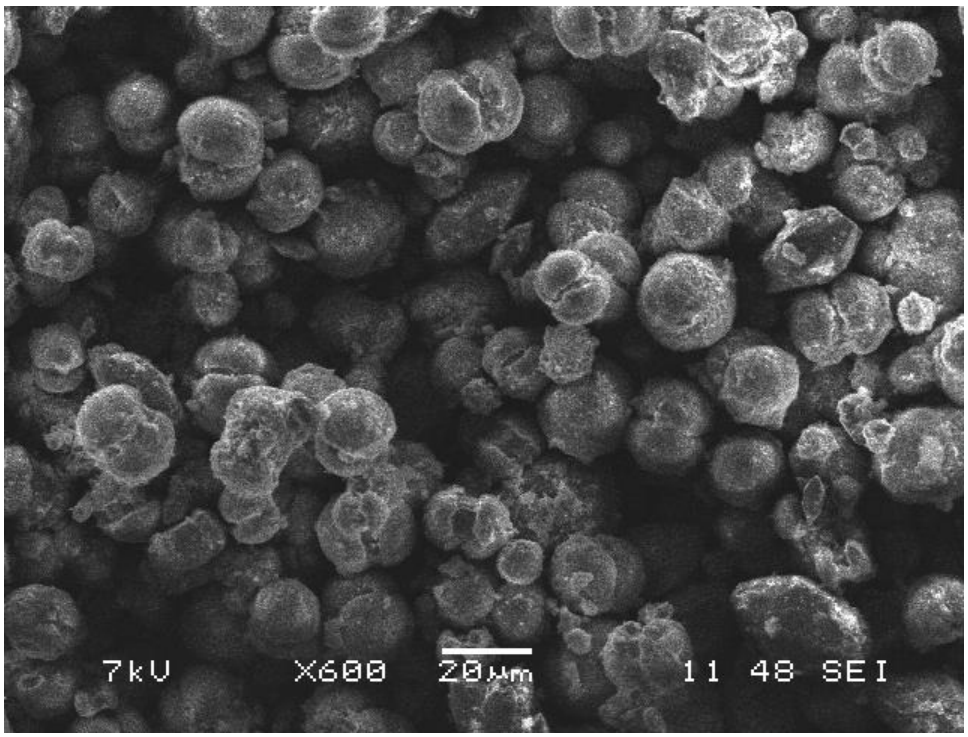

Figure S9: SEM image of MgAlPO-5.

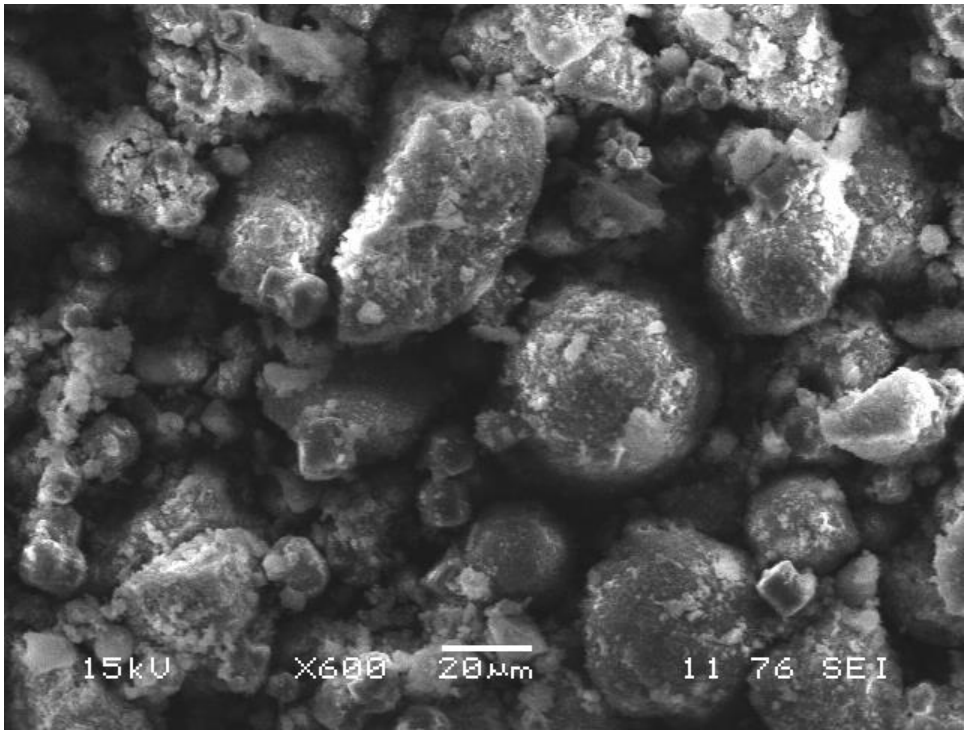

Figure S10: SEM image of SiAlPO-5.

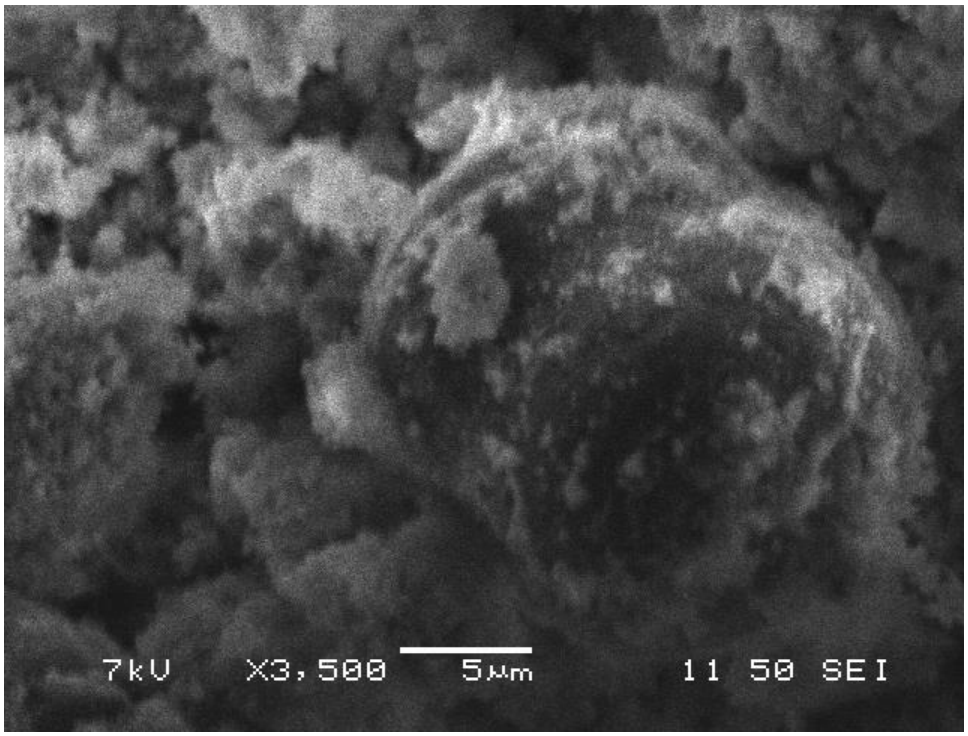

Figure S11: SEM image of MgSiAlPO-5.

Table S4: Summary of TPD data

Sample	150-200 °C	200-300 °C	300-400 °C	400-500 °C	500-600 °C	Total
SiAlPO-5	0.002	0.047	0.044	0.030	0.015	0.138
MgSiAlPO-5	0.001	0.041	0.044	0.018	0.017	0.121
MgAlPO-5	0.001	0.054	0.093	0.052	0.030	0.229

The MgSiAlPO-5 and SiAlPO-5 catalysts have a comparable fraction of acid sites, whilst the MgAlPO-5 possesses a much higher density of strong acid sites. However, we believe that the type of substrates used in this study (cyclohexanone oxime and benzene) bear little resemblance to the NH3 probe that has been used in the TPD measurements and, as such, it is difficult to ascertain subtle differences between the MgSiAlPO-5 and SiAlPO-5 catalysts on the basis of purely the NH3-TPD data. In light of this, we have resolved and quantified the signals observed using the 2,6-DMP probe (Table 2 on page 5 in the main paper, and Figure S12 below). This shows the subtle differences in acid site strength that exists between the two catalysts and more importantly highlights the differences in the quantity of accessible active (acid) sites.

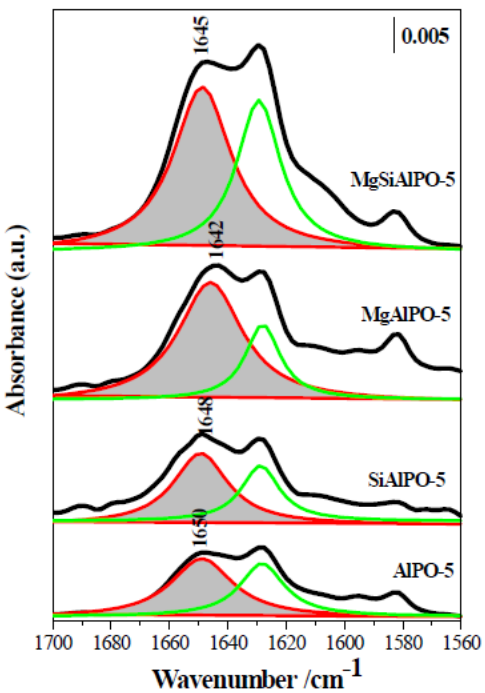

Figure S12: FTIR spectra of outgassed 2,6-DMP at 298K on mono- and bi-substituted AlPO-5 catalysts. Red and green lines: simulated spectra obtained by a curve fitting procedure.

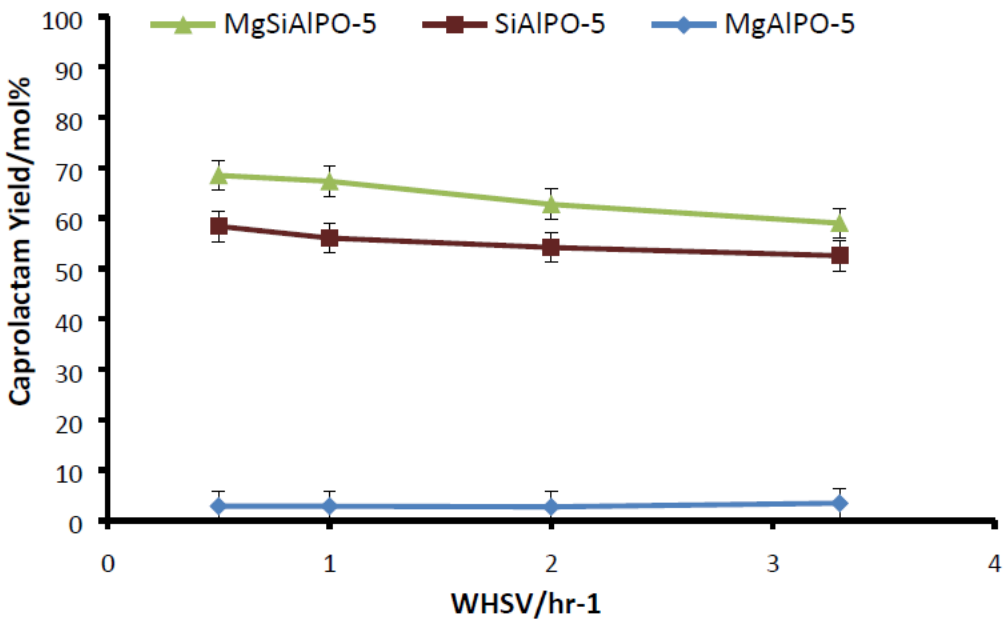

Figure S13: Caprolactam yield versus WHSV.

Carbon balance

The feed solution for assessing the carbon balance using chlorobenzene as the internal standard was composed of:
Chlorobenzene: 2.9929 g (0.026589 mol)
Cyclohexanone oxime: 15.0088 g (0.132633 mol)
Made up to 50 ml with methanol (solvent).

Response factor for Cyclohexanone oxime relative to Chlorobenzene = 1.2972 (Calibrated)
Response factor for Caprolactam relative to Chlorobenzene = 1.4516 (Calibrated)
Response factor of Others relative to Chlorobenzene = 1

Performing an identical procedure to the one described above the following GC data was obtained at 673 K, WHSV of 3.3 hr-1:

Time/mins	**Molecule**	**Area**
2.7	Chlorobenzene	233780.63
4.1	Cyclohexanone oxime	216732.37
5.9	Caprolactam	489031.09
N/A	Others detected by GC	119505.20

Rearranging: Moles of A/Moles of B = RF x (Area of A/Area of B)
Gives: Moles of A = Moles of B x RF x (Area of A/Area of B)

Using the equations and response factors above the moles of the remaining molecules can becalculated by normalisation to the internal standard (0.026589 moles).

Time/mins	Molecule	Area	Moles
2.7	Chlorobenzene	233780.63	0.026589
4.1	Cyclohexanone oxime	216732.37	0.031976
5.9	Caprolactam	489031.09	0.080739
N/A	Others detected by GC	119505.20	0.013592

Conversion = 100 x (Initial moles of oxime – Moles of oxime)/Initial moles of oxime
Conversion = 75.9 mol%

Selectivity = 100 x (Moles of Lactam)/Moles of converted oxime
Selectivity = 80.2 mol%

Yield = 100 x (Moles of Lactam)/Initial moles of oxime
Yield = 60.9 mol%

Mass balance = 100 x (Moles of [Oxime + Lactam + Others])/Initial moles of oxime
Mass balance = 95.2 mol%

Both the reproducibility and carbon balance (>95 mol%) are within accepted limits.